Origins of Linear Viscoelastic Behavior of Polymer−Nanoparticle Composites

Victor Pryamitsyn and Venkat Ganesan*

Department of Chemical Engineering, University of Texas at Austin, Austin, Texas 78712

Received August 21, 2005; Revised Manuscript Received November 9, 2005

ABSTRACT: We use computer simulations to study the mechanisms governing the linear viscoelasticity behavior of composites of spherical nanofillers dispersed in polymer melt matrices. Our results suggest that particles can influence the viscoelastic properties of the system by a variety of different mechanisms. On one hand, the particle-induced effects on the dynamics of polymer segments modify the relaxation spectrum of the polymers. Second, particle jamming effects lead to slow relaxations and substantial enhancements in elasticity. Finally, our results suggest that the strain field distortion caused by the presence of rigid inclusions also affects the overall modulus of the composite. For our model system, we delineate the regimes and frequencies at which the different effects manifest and also suggest how the picture can be generalized for parametric conditions different from our simulations.

Mixtures of polymers and particles occur in a variety of practically important applications such as paints, coatings, and rheological modifiers.[1,2] In many of these applications, the polymer size (i.e., the length scale controlling polymer physics, denoted in this article as R_g) is much smaller than the size of the particle R. This limit, termed the "colloid" limit, is also the regime which has seen many advances in models and simulation approaches for predicting the equilibrium and dynamical properties of polymer−particle mixtures.[3] More recent applications have involved polymer−particle mixtures in the "nanoparticle limit", where the size of the polymer is comparable to or larger than the particle size. For instance, in materials broadly termed as polymer nanocomposites (PNCs), nanoparticles of different shapes with sizes in the range 5−50 nm (comparable to R_g) are routinely dispersed in polymeric matrices to enhance their properties.[4−6] Many such efforts are motivated by experimental observations which have suggested that at loadings where modest property enhancements were reported for colloidal particles either significant or novel property enhancements can be attained for nanoparticle fillers.[4−6] However, efforts to translate these observations to systematic strategies have brought forth many new physical aspects and challenges highlighting the subtleties of the nanoparticle limit. For instance, for equilibrium properties, features such as the curvature of the particle relative to the polymer size, polymer−filler interactions, and the filler−filler interactions have all been shown to play an important role in determining the dispersion stability and thermodynamic behavior.[7−10] At a dynamical and/or rheological level, where much progress was made in the colloid limit by modeling the polymer matrix as a structureless continuum non-Newtonian fluid,[11] experiments have clearly suggested a breakdown of this "continuum-solvent" wisdom in the nanoparticle regime.[12]

The successful fruition of applications involving PNCs depends on their processability, which in turn is dependent on understanding and controlling their flow behavior. Not surprisingly, the rheological behavior of PNCs has attracted significant attention,[4−6,13−23] and a number of intriguing phenomena have been observed. In the present article we focus on the linear viscoelasticity characteristics of the PNCs. Many experimental measurements of the linear viscoelastic properties of PNCs have suggested that PNCs display strong enhancements in the elasticity (plateau modulus) with increasing concentrations of the particulate phases.[14,15,17,20,21] Moreover, in a number of systems, the latter has manifested in almost a solidlike behavior with a plateau in the storage modulus $G'(\omega)$ persisting at even extremely low frequencies.[14,17−19,21] While the experimental results have been quite generic, physical explanations of these phenomena have been somewhat divided. Early observations of the solidlike behavior have rationalized it as a purely particle phenomena, viz., arising from the jamming of the (highly anisotropic) particulate phases.[14,17,21] The latter was speculated to arise upon exceeding the percolation or the glass transition thresholds for loading of the fillers. More recent observations (and simulations) have suggested that polymer−particle interactions can also lead to such effects.[18,19,24,25] The latter can arise either due to enthalpic interactions or physicochemical heterogeneities which leads to significant reductions in segment mobility near the particle surfaces.[26−30] It has been proposed that in such instances the polymer segments can be "immobilized" near the particles, leading to the formation of particle-mediated transient polymer networks which can result in significant enhancements in elasticity.[18,24,25] Finally, a third mechanism, with origins in continuum mechanics, has also been suggested for the above effects. Indeed, just the addition of microscopic filler particles to polymer matrices results in a distortion in the applied strain fields, leading to an enhancement in the macroscopic viscoelastic properties of the composite.[31−36] The latter effects could also in principle lead to complex rheological responses when considered for the PNC system.

In this article we use computer simulations to address the questions: "How do nanoparticles modify the viscoelastic behavior of polymer matrices?" "What are the mechanisms underlying these influences?" "What parameters govern these mechanisms?" To this objective, we consider a somewhat idealized, albeit well-characterized, model system, viz., one involving hard, spherical nanofillers well-dispersed in unentangled polymer melt matrices to delineate the physics governing the linear viscoelasticity behavior of PNCs. By choosing the model of spherical fillers, we take advantage of the fact that much is known about the equilibrium and dynamics of spherical

* Corresponding author. E-mail: venkat@che.utexas.edu.

10.1021/ma051841z CCC: $33.50
Published on Web 12/16/2005

particles in viscous and elastic media. For instance, the percolation threshold for random packing of spheres (cf. also discussion in section 2) is expected around $\phi_p = 0.3$;[37−39] the glass transition occurs around $\phi_g = 0.58$.[40,41] Moreover, at a continuum level the influence of spherical particles on the viscosity and elasticity of the suspension is well-understood.[3,42,43]

To place our study in the context of applications, we briefly discuss the parametric conditions accompanying our study and their relationship to experimental situations. Viscoelastic properties of PNCs are controlled by the interplay between three length scales: the filler size R, the polymer size R_g, and the interparticle distance d. We note that earlier pioneering studies by Smith,[44] Glotzer,[45] and Kumar[24,46] and co-workers have examined different aspects of this parameter space. Of these, we note that the seminal study of Smith and co-workers[44] considers issues closest related to our work, albeit the parameters and analysis methodology employed are different. Experimental situations involve $R/R_g \simeq O(1)$ for systems such as laponites[13] and silica nanoparticles to $R/R_g \simeq 10-50$ for montmorillonite clays.[14] While we cannot simulate this wide a spectrum of polymer and particle sizes, the results presented in the subsequent sections consider different polymer sizes such that $R/R_g \simeq 0.5-2.5$. Further, we consider only cases of nonagglomerated, well-dispersed (exfoliated) particles where the definition of the filler size R is unambiguous. Second, in most PNC systems, almost all interesting rheological effects have been observed in the regime where the interparticle distance d satisfies $d/R_g \lesssim O(1)$. To capture latter effects, we consider a range of nanoparticle volume fractions and polymer sizes such that the extreme situation of the longest polymers in the densest suspension corresponds to the interparticle distances $d/R_g \simeq 0.1$. To probe such regimes, the use of a spherical nanoparticle necessitates us to use volume fraction ranges (loadings) significantly higher than those used in experiments.[14,18,19]

Our simulation methodology (elaborated in the next section) is a coarse-grained approach and does not account for the entanglement effects between polymers. This feature contrasts with many experimental situations involving PNCs. However, we anticipate that many of the qualitative conclusions presented in the following sections will remain equally valid for entangled systems, with the possibility that a more richer phenomenology can manifest in entangled systems due to the influence of additional time and length scales controlling the dynamics of the polymer. Second, we also consider energetic interaction parameters representative of a well-compatiblized nanocomposite melt where particle aggregation is minimized. Broadly, the sign of polymer-mediated interaction between the particles depends on whether the local density of the polymer melt at particle−polymer interface is lower or higher than the bulk density of the polymer melt. In the first case it leads to depletion attraction (and possibly aggregation), whereas in the second case it leads to an accumulation−repulsion (and stabilization). We have tuned the polymer−particle interaction to provide the interfacial density of polymer melt to be high than the bulk value to prevent aggregation. Such a method was used earlier in our simulation of colloid particles in simple fluids[48] where the absence of aggregation was verified by the calculation of the particle−particle pair correlation function.

Within the above model, we use a combination of computer simulation results, models, and scaling arguments to examine the relative roles of polymer mobility reduction and the particle interactions for the enhancement in the linear viscoelastic properties of the polymer matrix. The former is directly incorporated in our model through a reduced polymer segment mobility near the particles, and the latter is accounted naturally through the interparticle interactions. As an outcome, we present the proposal that all three mechanisms discussed earlier contribute to the viscoelastic properties of PNCs. The polymer mobility effects manifest at lower particle loadings, and we show that the formation of a strict network requires a significant slowing down of the polymers. More importantly, our results suggest that the formation of such a network is not a necessity for the enhancement in viscoelastic properties. Rather, the particle-induced changes in polymer dynamics can even otherwise lead to important effects on the linear viscoelastic properties. Second, we demonstrate that particle interactions also play a significant role, albeit manifesting only at higher particle loadings. In the latter regard, we suggest that the resulting effects are more similar to the behavior of colloidal suspensions near glass transition. Finally, we present more speculative evidence that the strain-field distortion-induced enhancement also plays a role, albeit at higher frequencies.

The rest of the article is arranged as follows: In section 1 we present an overview of the simulation approach. Most of the details and parameters are relegated to the Appendix. In section 2 we present our results for the linear viscoelastic behavior of PNCs. In sections 3.1 and 3.2 we discuss the mechanisms underlying the oscillatory shear results. In section 4 we present the results of a modified Rouse model to mimic and study the relative effects of transient network formation and particle jamming. In section 5 we present our conclusions with an outlook for future work.

1. Simulation Details

In our simulations, we consider a model of spherical nanofillers of a fixed size (the radius denoted $R = 2.5$ units) dispersed at different loadings (ϕ) in a coarse-grained model of polymer matrices of different chain lengths N_P. The R_g of the polymer ranges from 1.7 units for $N_P = 8$ ($R_g/R = 0.7$) to 6.0 units for $N_P = 96$ ($R_g/R = 2.4$). A weak attractive interaction exists between the nanoparticle and the polymer segments such that direct particle−particle aggregation is eliminated. The equilibrium and dynamics of this system are simulated by a recently proposed variant of the dissipative particle dynamics (DPD) approach.[47,48] An earlier publication[48] used the above simulation method to simulate the dynamics of spherical particles in simple fluids and demonstrated excellent agreement with both experimental results and alternate theoretical approaches. For the present work, we make minor modifications to the conservative forces and parameters (in addition to the dissipative forces mentioned below) to account for the polymeric nature of the solvent. In the following we make two comments regarding the simulation and present a summary of the method and the simulation parameters in the Appendix.

The simulation approach proposed[48] was based on the idea of the fluid particle model developed by Espanol[49,50] and modifies the dynamical equations of motion to admit shear forces to be transmitted between the simulation moieties. The latter mimics the frictional forces arising due to the relative movement of the coarse-grained simulation units. In the present work, we use this framework to directly incorporate the particle-induced effects on the polymer mobilities. This model is chosen to mimic experimental observations which have suggested that the mobility of the polymer segments near solid interfaces tend to be much lower than in the bulk. In an unfunctionalized polymer melt, the exact origin of this effect is still unresolved but is speculated to be due to[30] the increases in the glass transition temperature which results due to the weak increases

in density that results near the surface (the increases in the density are necessarily small due to the highly incompressible nature of the melt). Second, physical and chemical heteorgeneities of the solid surfaces have also been shown to cause a significant slowing of the polymer monomers.[30]

In our coarse-grained simulation model, we do not have access to the glass transitions of the polymer, nor is simulating physicochemically rough particles computationally feasible. As an indirect approach to mimic the above particle effects on polymer segment mobility, we introduce an enhanced tangential friction force between colloid particle and the polymer segments within the framework of the fluid particle model. Explicitly, we choose our parameters such that the polymer segments experience an enhanced particle-induced friction (denoted γ_{CS} in the Appendix) compared to the segment−segment friction (γ_{SS}) in the bulk matrix. Because of simulation time and efficiency constraints, we are able to mimic only relatively weak mobility changes for the polymers near the particles. A comparison of the reduction in mobilities to the simulations of Smith et al.[30] suggests that our values are reasonable in mimicking the effects observed near an adsorbing interface but is much weaker than the effects observed near a heterogeneous surface. Whence, we complement our simulations with the results of a schematic dynamically quenched Rouse model (section 4) which allows us to discuss the phenomena which might manifest in the regime of strong mobility changes.

Simulation approaches commonly use the Kubo formula[44,51,52] to discern the linear viscoelastic properties. However, recent work by Barrat and co-workers[53] have demonstrated that such an approach is extremely error prone (unless long computational trajectories are used) and have cautioned against its usage for systems involving polymeric components. Preliminary runs for our system appeared to confirm some of the arguments advanced by Barrat, and so we opted to extract the linear viscoelastic properties by a direct simulation of the oscillatory shear using the nonequilibrium method outlined in Allen and Tildesley.[54] The details of the latter are also presented in the Appendix.

2. Linear Viscoelasticity: Oscillatory Rheology

In this section we present the results for the linear viscoelasticity of the PNC system obtained by imposing an oscillatory strain. The strain, γ_0 was maintained at a value of 0.1, which was verified to be in the linear regime of the viscoelastic response. In this section, we mainly present the results and comment on their consistency with experimental observations. In subsequent sections, we discuss the mechanisms underlying the observations.

We first comment on the behavior expected for the pure polymer matrix. The coarse-grained simulation approach employed in this work uses soft interaction potentials between the polymer segments and hence cannot capture the entanglement effects of a polymer matrix.[55] Consequently, we expect the dynamical response of a pure polymer matrix containing no particles to follow the Rouse behavior.[55,56] In such cases, the linear viscoelasticity spectrum for the storage modulus $G'(\omega)$ is expected to show three characteristic regimes[56] separated by the monomer relaxation times (denoted τ_0) and the longest relaxation time τ_N (which for Rouse polymers scales as $\tau_0 N^2$). At the highest frequencies $\omega > \tau_0^{-1}$, $G'(\omega)$ displays a plateau reflecting the lack of relaxation processes on such time scales. At intermediate frequencies, corresponding to $\tau_N^{-1} < \omega < \tau_0^{-1}$, $G'(\omega) \sim \omega^{1/2}$, reflecting the Rouse relaxation spectrum of the polymer. Finally, for $\omega < \tau_N^{-1}$, the terminal relaxation behavior sets in and $G'(\omega) \sim \omega^2$.

Figure 1a−d presents the main results of this work, viz., quantifying the influence of the particles on the storage modulus $G'(\omega)$ of the polymer matrices. The results displayed pertain to PNC matrices of different chain lengths N_P of the matrix polymer at four different particle concentrations ϕ ranging from dilute to the concentrated regimes. Our simulations probed the same range of frequencies for the different matrices, and hence the dynamical response corresponds to distinct relaxation regimes for the different polymers. Indeed, it is evident that for $N_P = 8$, 24, and 48 we probe parts of the Rouse and terminal regimes, whereas for $N_P = 96$ we probe the Rouse regime of relaxation.

The results corresponding to $\phi = 0.007$ are expected to closely approximate the behavior of a pure polymer matrix and hence provide a comparison for studying the particle-induced effects. From the results of Figure 1, we observe that the particles have qualitatively distinct effects depending on the volume fraction of loadings. At low particle loadings ($\phi = 0.11$ and 0.33), the qualitative features (shapes) of the viscoelastic behavior are unaffected by the addition of the nanoparticles. At a quantitative level, the particles lead to an increase in the magnitudes of the storage modulus $G'(\omega)$ (i.e., reinforces the matrix) at all frequencies. Indeed, for $\phi = 0.33$, we observe that the magnitudes of the particle-induced enhancement becomes significant [$O(5-10)$] at the low frequencies. On the other hand, at the highest particle loading of $\phi = 0.5$, we observe that the characteristic relaxations are dramatically slowed and evolve from the Rouse-like behavior to a solidlike relaxation ($G'(\omega) \sim \omega^{\alpha}$, $\alpha \ll 0.5$) at the lowest frequencies. The latter effect concomitantly leads to an extremely significant contribution to the elasticity, where 3−4 orders of magnitude enhancements in $G'(\omega)$ relative to the pure polymer matrix can be noted.

To corroborate the qualitative changes that occur between the lowest and the highest particle loadings, in Figure 2a,b, we present the frequency dependence of tan $\delta(\omega) = G''/G'$ for matrices with $N_P = 24$ and 48. The latter quantifies the relative contributions arising from the viscous and the elastic components of the rheological response,[56] and for viscoelastic fluids tan $\delta \to \infty$ as $\omega \to 0$ (reflecting the viscous nature of the fluid) and tan $\delta \to 0$ as $\omega \to \infty$ (reflecting the elastic nature of the fluid), and slow, monotonic crossover between the above asymptotic behaviors at intermediate frequencies. From our results, it is again observed that at loadings $\phi = 0.007$, 0.11, and 0.33, the qualitative behavior of tan δ resembles that of the unperturbed polymer matrix and exhibits a viscous behavior as $\omega \to 0$. In contrast, at the highest particle loading of $\phi = 0.5$, it is observed that tan δ adopts a positive slope at low frequencies, indicating a transition from the viscous behavior to a solidlike behavior.

The above trends in viscoelastic behavior are qualitatively consistent with experimental observations and already provide some insights into the mechanisms. Many experimental results have suggested that the viscoelastic behavior at the high frequencies qualitatively resembles the behavior expected for the pure polymer matrix.[14,17,21] This observation is borne out in our simulation results and is seen to be true even at the highest particle loading $\phi = 0.5$. With an increase in particle loading, a number of experiments have reported an enhancement in the elasticity and the development of a solidlike plateau in $G'(\omega)$—a result consistent with our simulation trends.[14,17−19,21]

In many studies, the qualitative changes observed in the viscoelastic properties have been speculated to arise from a percolation transition of the fillers. While an unambiguous

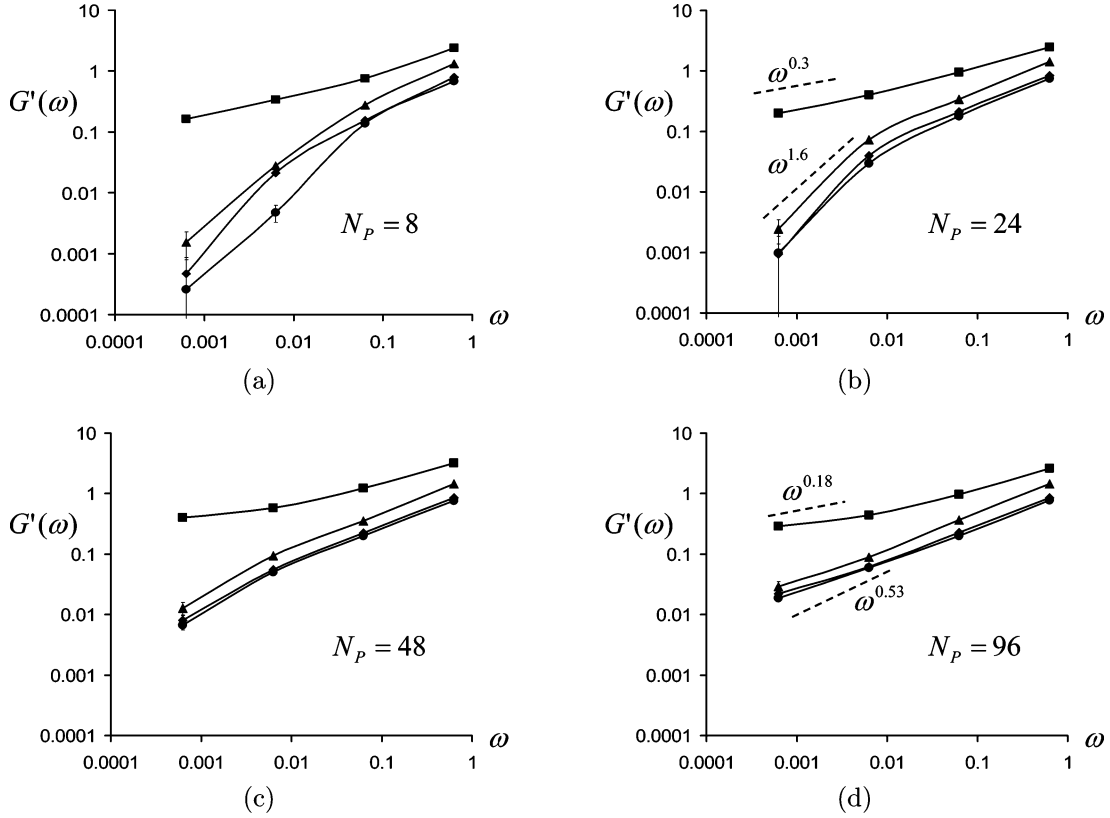

Figure 1. Storage modulus $G'(\omega)$ for polymer matrices of different chain lengths, N_P. The circles correspond to $\phi = 0.007$, diamonds to $\phi = 0.11$, triangles to $\phi = 0.33$, and squares to $\phi = 0.5$. Corresponding error bars are also displayed for all cases (in many instances, the errors are too small to be visible).

definition of percolation transition is not possible without a measure of "connectedness", by and large, theoretical results point to a percolation threshold of $\phi \sim 0.3$ for a wide range of such definitions.[37−39] Our results suggest that this percolation transition has no special significance for spherical particles, but rather, a much higher particle loading is necessary to achieve a qualitative change in the shape of the viscoelastic spectrum. The latter aspect of our simulations seems to contrast with experimental observations wherein extremely low loadings have led to such changes in the viscoelastic behavior.[14,17−19,21] While we address this issue in detail later, we note that most experiments involve highly anisotropic particles, where orientational constraints lead to jamming at much lower loadings.[56] In contrast, $\phi = 0.5$ is close to the volume fraction of $\phi_g = 0.58$ at which a suspension of hard, noninteracting spherical particles jams and forms a glass.[40,41] We suggest (and demonstrate later) that it is this relative distance from the jamming transition which determines the viscoelastic behavior.

In the subsequent sections, we examine the mechanistic underpinnings of the above results. Specifically, we address the following questions: (i) What are the mechanisms underlying the above particle effects on the viscoelastic behavior? (ii) What distinguishes the mechanisms at low and higher particle loadings? (iii) How parametrically general are our results and conclusions? Our approach will be motivated by the hypothesis that either the changes in polymer dynamics caused by the particles (transient network mechanism) and/or dynamics arising from particle−particle interactions could be leading to the above behaviors. As a tool to distinguish these characteristics, we consider the equilibrium dynamical characteristics of both the polymer and the particles in the PNC matrices at the different loadings and analyze their contributions to the linear viscoelasticity.

3. Origins of Viscoelasticity

A. Low Particle Loadings. In this section, we address the mechanisms underlying the viscoelasticity behavior noted for PNCs at low loadings. We recall that the main characteristics observed were a viscoelastic spectrum qualitatively similar to that of the pure polymers, with however a quantitative enhancement in the elasticity dependent on the particle loadings.

The first quantity we examined was the equilibrium dynamical characteristics (in the absence of any oscillatory strain) of the polymers through the relaxation spectra of the normal modes, $\mathbf{X}_p(t)$, of the polymer.[44,56,57] The normal modes of a polymer and its dynamics represent a sensitive measure of the dynamical characteristics of the individual polymers when examined at different length scales. For an unperturbed Rouse polymer, we recall that there are N_P normal modes which are defined through

$$\mathbf{X}_p(t) = \sqrt{\frac{2}{N_P}} \sum_{i=1}^{N_P} \cos\left(p\pi \frac{i - {}^1/_2}{N_P}\right) \mathbf{R}_i(t) \qquad (1)$$

where p is the mode index ($1 \le p \le N_P$) and $R_i(t)$ denotes the position of the segment i at time t. Moreover, these normal modes relax by a single-exponential decay of the form $\langle \mathbf{X}_p(t) \cdot \mathbf{X}_p(0) \rangle \simeq \exp(-t/\tau_p^R)$, where the relaxation times τ_p^R form a spectrum:[56,57]

$$(\tau_p^R)^{-1} \propto \frac{12}{\xi b^2} \sin^2\left[\frac{\pi p}{2N_P}\right], \quad p = 1...N_P \qquad (2)$$

with ξ representing the segmental friction coefficient.

In the presence of particles, the above Rouse behavior of the polymers can be modified in two distinct ways. On one hand, the relaxation of the normal modes could still remain a single

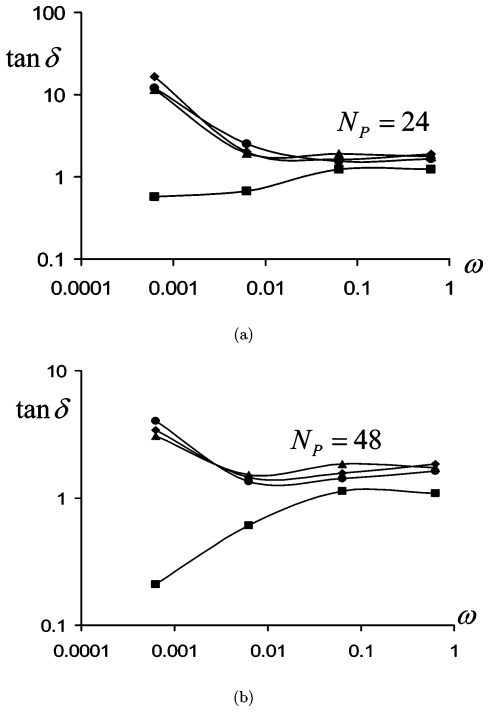

Figure 2. Behavior of tan δ for $N_P = 24$ and 48. The circles correspond to $\phi = 0.007$, diamonds to $\phi = 0.11$, triangles to $\phi = 0.33$, and squares to $\phi = 0.5$.

exponential of the form $\langle \mathbf{X}_p(t)\cdot\mathbf{X}_p(0)\rangle \simeq \exp(-t/\tau_p)$, but with however a modified relaxation spectrum τ_p reflecting the influence of the particles. The latter is indicative that the dynamics of all the polymers are equally affected (termed as "homogeneous" dynamics) but that the individual relaxation dynamics of the polymers are modified at or beyond certain length scales. A similar effect manifests for instance in the transition from the Rouse to entangled behavior in polymer melts, where the relaxation times of modes $p < N_P/N_e$ (where N_e denotes the entanglement length of the polymer) are modified due to entanglement effects.[58] A second scenario for particle impact arises when the relaxation of the normal modes no longer satisfies a simple exponential decay, but rather decays through either a stretched exponential or multiple exponential decays. The latter is a manifestation of "heterogeneous" dynamics, wherein the relaxation reflects the dynamics of distinctly relaxing elements, each of which relaxes at widely separated and/or with a different rates.[59−61] Such a situation could occur if only some of the polymers form a network, when their dynamics is effectively frozen on the time scale the free polymers are themselves relaxing.

In Figure 3, we present the results of the relaxation of normal modes $X_p(t)$ for the polymer matrix $N_P = 96$ at particle loadings $\phi = 0.007$ and $\phi = 0.3$. The Appendix details the procedure used for determining these spectra. Also indicated in Figure 3 are the parameters of a stretched exponential fit of the form $\exp[-(t/\tau_p)^\beta]$ for the relaxation of the first few modes. The exponent β (i.e., its deviation from unity) characterizes the nonexponentiality of the fit and the "heterogeneous" nature of dynamics.[59−61] The first observation we make from Figure 3 is that at both the loadings ($\phi = 0.007$ and $\phi = 0.33$) the relaxation dynamics of the normal modes do, to a good approximation, follow a single-exponential decay. This observation suggests that at low loadings it is not a polymer network formed by a few chains that is responsible for the effects observed in the viscoelastic properties.

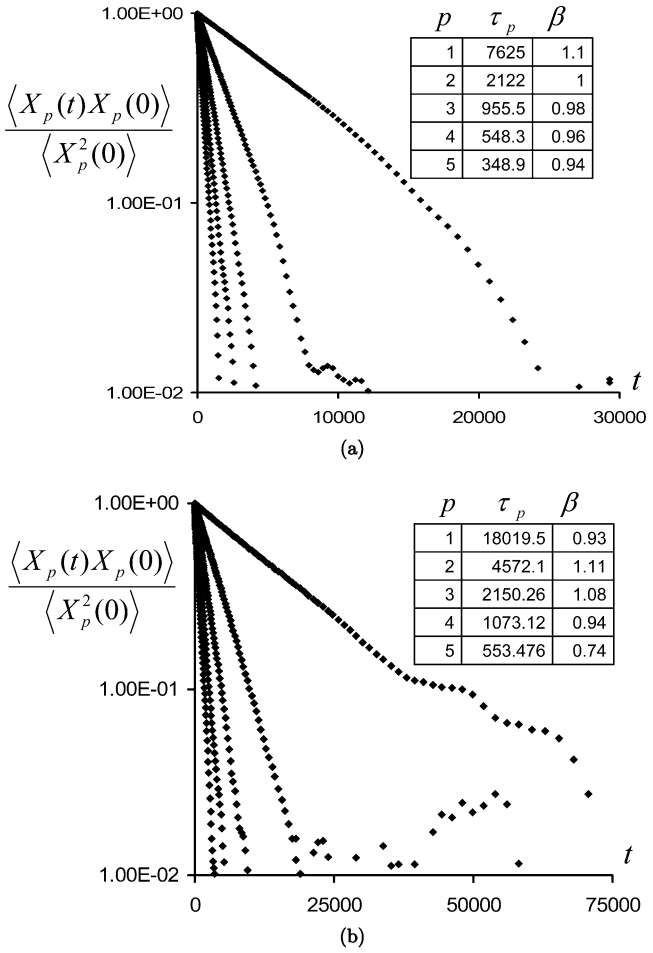

p	τ_p	β
1	7625	1.1
2	2122	1
3	955.5	0.98
4	548.3	0.96
5	348.9	0.94

p	τ_p	β
1	18019.5	0.93
2	4572.1	1.11
3	2150.26	1.08
4	1073.12	0.94
5	553.476	0.74

Figure 3. Relaxation of normal modes X_p for matrix $N_P = 96$. Only the relaxation of the modes $p = 1-5$ are displayed: (a) $\phi = 0.007$; (b) $\phi = 0.33$. The table represents the fits to a stretched exponential function of the form $\exp[-(t/\tau_p)^\beta]$.

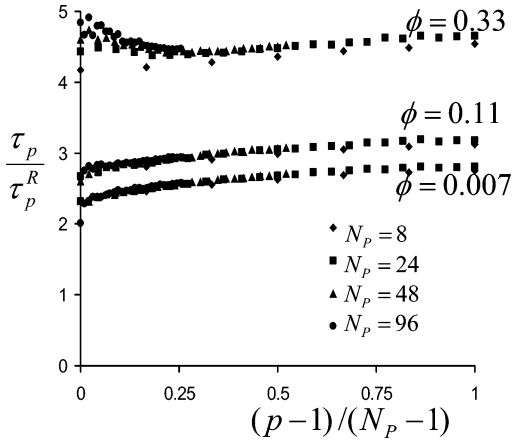

Figure 4. Relaxation times τ_p normalized by $(\tau_p^R)^{-1} = \sin^2(\pi p/2N_P)$ of normal mode p for matrices of different N_P.

The effect of the particles can be rationalized by considering their impact on the relaxation times τ_p of the polymer modes. To quantify this effect, in Figure 4 we display the normalized relaxation time $\tau_p \sin^2(\pi p/2N_P)$ for the chains of different matrix N_P's at loadings corresponding to $\phi = 0.007$, 0.11, and 0.33. We observe that, to an excellent approximation, the relaxation times all collapse approximately onto a particle loading dependent constant value. The latter suggests that in the PNC matrices the polymers still follow a Rouse spectrum, albeit with a concentration-dependent shift in the magnitudes of all the

relaxation times. Overall, the observed behavior can be rationalized by noting that in our simulations the segments exhibit a reduced mobility near the particle surfaces. At low loadings and for the weak mobility changes incorporated in our simulations, the polymers are not permanently "immobilized" near the particles. Rather, within the longest relaxation time of the polymer, different segments are able to access the lower mobility regions, leading to a slowing down of the overall dynamics of the polymer segments. Addition of more particles creates more polymer−particle interfaces which enhances this effect and leads to a further increase in the relaxation times. We do note that small deviations from the Rouse behavior are evident for $\phi = 0.3$—we return to this aspect in the next section where it becomes more pronounced.

The above conclusion is qualitatively consistent with our results of previous section obtained using the oscillatory strain. Indeed, a concentration dependence of the segmental friction coefficient would lead to a shift of the viscoelastic relaxation spectra for the polymers. The latter could in part explain the enhancements in the storage modulus (at a given frequency) observed in Figure 1. So we consider whether the overall viscoelastic behavior could be completely rationalized by this effect. For this purpose, we use the classical relationship[56] between the equilibrium dynamical characteristics and the linear viscoelasticity and use the above-determined relaxation times of the polymer τ_p to compute the "polymer component" of the storage modulus (expressed in units of k_BT) through[56,57]

$$G_{pol}(t) = \frac{\rho_p}{N_p}\sum_{p=1}^{N_p-1}\frac{\langle \mathbf{X}_p(t)\cdot\mathbf{X}_p(0)\rangle^2}{\langle \mathbf{X}_p(0)\cdot\mathbf{X}_p(0)\rangle^2} \quad (3)$$

where ρ_P represents the polymer density expressed in number of segments per unit volume. The above equation is applicable when the relaxation dynamics of the polymer is "homogeneous", an assumption which is reasonable considering our earlier fits based on the stretched exponentials.

In Figure 5a, we present a comparison of the $G'(\omega)$'s extracted from the oscillatory shear data (Figure 1) and $G'_{pol}(\omega)$. Note that $G_{pol}(t)$ represents the linear viscoelasticity shear modulus arising from the polymer dynamics and its relaxation and embodies the influence of the particles only in their effects upon the relaxation dynamics of the polymers. In contrast, $G'(\omega)$'s extracted from the oscillatory shear include the contributions to the storage modulus arising from the nanoparticles. We observe that at low frequencies and/or low loadings there is a quantitative match between $G'(\omega)$ and $G'_{pol}(\omega)$ (we note from Figure 1) that the numerical errors tend to be higher at extremely low frequencies). In contrast, at higher frequencies, it is evident that there are deviations between $G'(\omega)$ and $G'_{pol}(\omega)$. The latter is more clearly illustrated in Figure 5b, which displays the ratio $G'(\omega)/G'_{pol}(\omega)$ from our simulations as a function of the frequency for $\phi = 0.11$ and 0.33. We again observe that at low frequencies the ratio approaches unity independent of the matrix loading and N_P. However, at higher frequencies deviations are evident, with the magnitude of deviations increasing with an increase in the particle loading ϕ. Whence, we conclude that while the overall shape, the qualitative features, and the quantitative values of the low-frequency behavior of $G'(\omega)$ can be accounted for by $G'_{pol}(\omega)$, an additional mechanism arising from the particle-induced stresses should lead to a frequency- and loading-dependent enhancement in the storage modulus $G'(\omega)$.

We speculatively suggest that the high-frequency characteristics of $G'(\omega)$ can be accounted by the additional stresses arising

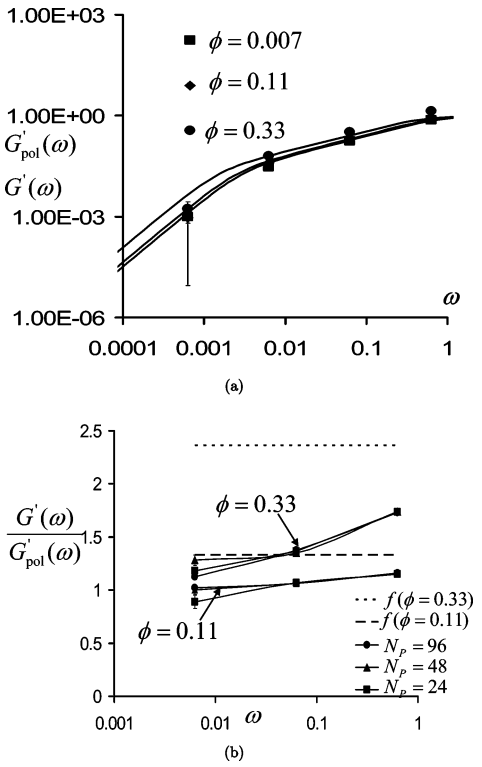

Figure 5. (a) A comparison of $G'(\omega)$ (points) and $G'_{pol}(\omega)$ (dotted lines) for matrix $N_P = 24$ and different loadings ϕ. (b) The frequency dependence of $G'(\omega)/G'_{pol}(\omega)$ for matrices with different N_P's. The dotted lines correspond to the continuum predictions for $\phi = 0.11$ and 0.3.

from the distortion of the strain fields produced by the presence of the particles. The latter effect underlies many continuum mechanical theories for the effective rheological and mechanical properties of a polymer−particle composite.[33−36] At the simplest level, these theories assume a perfectly bonded interface between the matrix and the rigid inclusion and predict an effective complex modulus $G^*_{cont}(\omega)$:

$$G^*_{cont}(\omega) = G^*_{matrix}(\omega)f(\phi) \quad (4)$$

where $G^*_{matrix}(\omega)$ denotes the bare (or particle-free) viscoelastic properties of the matrix and $f(\phi)$ is the enhancement in the modulus arising from the inhomogeneous strain field created by the presence of the inclusions.

We suggest that the above equation should incorporate two modifications to model the effective modulus of PNC systems. On one hand, the particle-free viscoelastic properties of the matrix should be replaced by the particle modified viscoelastic properties of the polymer matrix $G^*_{pol}(\omega; \phi)$ (with the ϕ dependence reflecting ϕ dependent nature of the particle effects themselves). Second, neither simulations nor experimental conditions satisfy the assumption of a perfectly bonded matrix.[36] In contrast, the segmental residence time near the interface also indirectly controls the stress transfer efficiency of the matrix. If we denote the latter, matrix chain length independent quantity as τ_S, we deduce that for frequencies $\omega\tau_S < 1$ the strain in the matrix does not feel the rigid particle. In contrast, for $\omega\tau_S > 1$ the strain field around the particle is distorted, leading to an additional source of elastic energy. Whence for imperfectly bonded matrices, we expect a frequency-dependent enhancement in the $G'(\omega)$ which can become very small at low ω. Together, these effects suggest an empirical equation of the form $G^*_{cont}(\omega) = G^*_{pol}(\omega;\phi)f(\phi,\omega)$, where f

(ϕ,ω) represents a frequency- and loading-dependent enhancement.

We note that several aspects of the above prediction and effect are consistent with the behavior in Figure 5b. First, the above contribution predicts that the enhancement in the storage modulus to be independent of the chain length N_P in terms of both its magnitude and its frequency dependence. We verify the above hypothesis for $G'(\omega)/G'_{pol}(\omega)$ in Figure 5b, which indeed accords with both these expectations. Second, in Figure 5b we compare the simulation results with the predictions of commonly employed continuum theory for filled polymers[35] where $f(\phi) = 1 + 2.5\phi + 4.94f^2$. It is apparent that at lower frequencies the observed enhancements are much smaller than the theoretical predictions and appear to approach the latter at asymptotically high frequencies, again in agreement with our above discussion on the frequency dependence of the boundary conditions.

In summary, this section considered the mechanisms underlying the viscoelastic behavior at low loadings. The particles were found to influence the observed characteristics in two distinct ways. On one hand, the particle−polymer interactions slow down the polymer segments near the surface, leading to a change in the relaxation spectrum and an enhancement in the modulus. This effect is the primary mechanism by which the low-frequency response is influenced and by itself leads to an order of magnitude enhancement in $G'(\omega)$. Second, the presence of rigid inclusions distort the strain field around the particles, leading to a frequency- and loading-dependent enhancement in the modulus. The latter contribution was more nominal in magnitude and was found to be relevant only for rationalizing the high-frequency behavior of our simulations.

B. High Particle Loadings. We recall that the viscoelastic response for the case of $\phi = 0.5$ exhibited markedly different characteristics. On one hand, the low-frequency behavior exhibited a plateau in the modulus. Second, the quantitative values of the enhancement in elasticity were substantial when contrasted with lower loadings. In this section, we consider different hypothesis to identify the mechanisms underlying the observed low-frequency viscoelastic behavior.

We begin by considering the particle-induced changes in polymer dynamics. In Figure 6a, we present the results for the relaxation dynamics of the normal modes $X_p(t)$ and the fits to the stretched exponential form $\exp[-(t/\tau_p)^\beta]$ for the matrix $N_P = 96$. Because of the much longer relaxation times entailed in these computations, we were unable to completely track the tails of the relaxation and eliminate the statistical errors. Despite this feature, by comparing the values of the β parameter presented in Figure 6a with that in Figure 3a,b, it is evident that increasing the particle loading has only a weak effect in rendering the polymer dynamics heterogeneous. This leads us to conclude that the stress relaxation mechanism underlying the viscoelastic behavior at $\phi = 0.5$ is not a phenomena ascribable to the dynamics of just a few networked polymer chains. This result is intuitive, since at particle loadings such as $\phi = 0.5$, it is very likely to find a particle surface next to some segment of every one of the polymers. Whence, dynamical effects are more likely to be homogeneous and manifesting on all the chains.

How do the particles influence the relaxation spectra? In Figure 6b we consider the functional form of the relaxation times τ_p of the normal modes. It is seen that the addition of particles has two distinct effects on the relaxation spectra. On one hand, similar to the behavior observed at lower loadings, we observe that the fastest relaxing modes (large p) are uniformly slowed down (i.e., the relaxation times τ_p are increased). On the other hand, for the slower relaxing modes (smaller p) a qualitatively new effect manifests as a deviation from the Rouse spectrum and a mode p dependent increase in τ_p. These deviations appear to be independent of N_P and occur for $p < p^*$ where $p^*/N_P \approx 0.4$. To rationalize these features, we recall that the latter behavior is strongly reminiscent of the characteristics of an entangled polymer, for which $\tau_p(p)$ follows the Rouse spectrum for $p/N_P < 1/N_e$ and modes $p/N_P > 1/N_e$ still follows the Rouse spectrum, albeit with relaxation times enhanced by a factor N/N_e.[57,58] Our results suggest that at higher particle loadings the particle-induced effects on the segment dynamics can in effect render the particles as "entanglements" for the polymer. The average entanglement length is now dictated by the loading dependent, but N_P independent, average interparticle distance. The increase in the relaxation times for modes $p < p^*$ can then be ascribed to the effective trapping of the polymer segments which occupy a length scale greater than the interparticle distance. We note that this mechanism also rationalizes the weak but noticeable deviations observed in the relaxation spectra for the slowest modes p at $\phi = 0.3$.

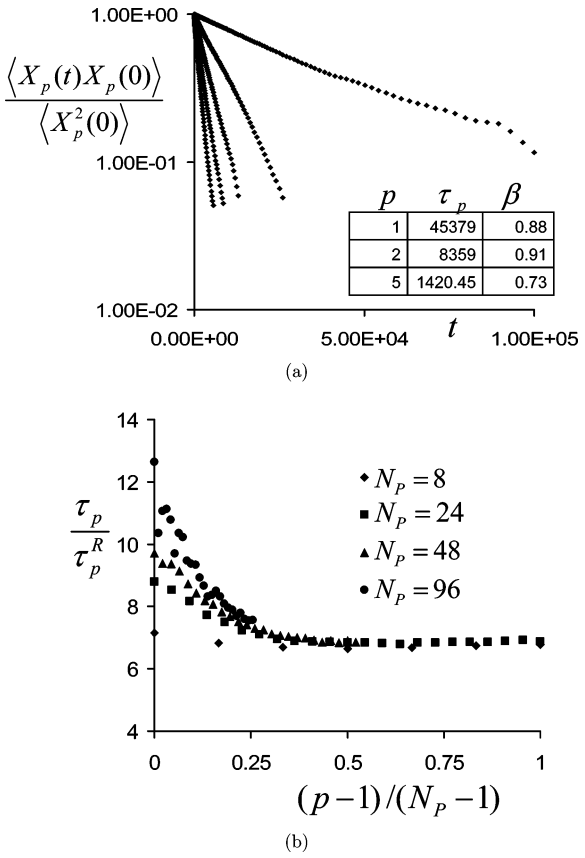

Figure 6. (a) Relaxation spectra of modes $p = 1-5$ for matrix $N_P = 96$ at $\phi = 0.5$. The table represents the fits to a stretched exponential function of the form $\exp[-(t/\tau_p)^\beta]$. (b) Relaxation times τ_p of normal mode p normalized by $(\tau_p^R)^{-1} = \sin^2(\pi p/2N_P)$ for matrices of different N_P at $\phi = 0.5$.

The question now is whether the above nontrivial effects on the normal mode relaxation spectra can quantitatively account for the viscoelastic behavior observed for the composite at $\phi_p = 0.5$. In Figure 7a we compare for the polymer matrices with $N_P = 8$, 24, and 96 the $G'_{pol}(\omega)$ obtained from the relaxation spectrum (using eq 3) along with the $G'(\omega)$ obtained from the oscillatory shear experiments. First, we observe that at a quantitative level the magnitudes of $G'(\omega)$ are significantly higher than the magnitudes of $G'_{pol}(\omega)$. On the other hand, even at a qualitative level we observe that $G'_{pol}(\omega)$ for $N_P = 8$ is in

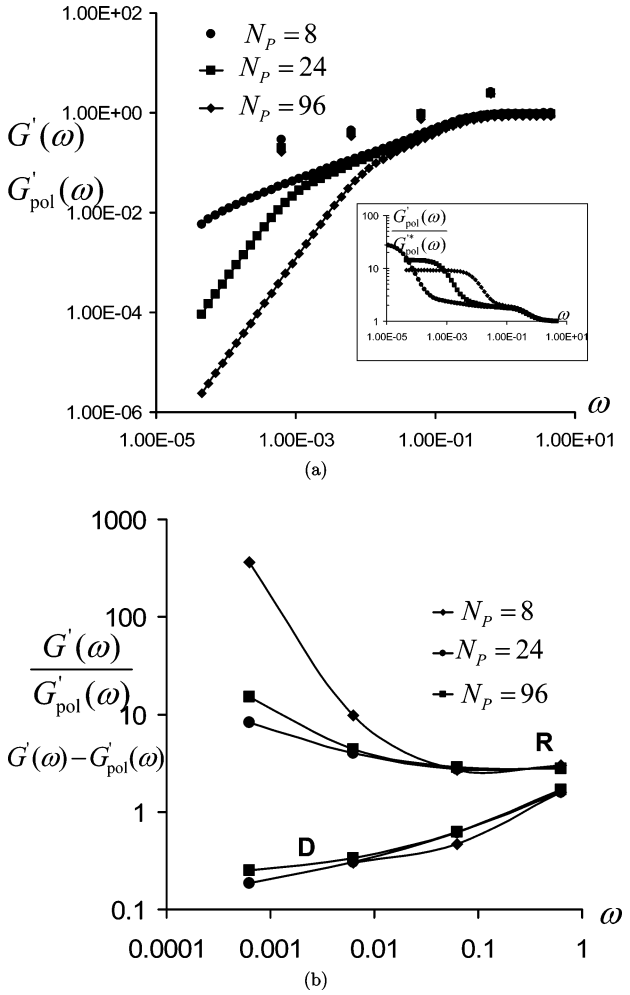

Figure 7. (a) A comparison of $G'(\omega)$ with G'_{pol} at $\phi = 0.5$. The points on the top represent the values of $G'(\omega)$ obtained in our oscillatory shear simulations, and the connected lines represent the G'_{pol} obtained using the equilibrium dynamical characteristics of polymers. Inset displays the ratio $G'(\omega)/G'_{pol}$ as a function of the frequency ω for the three chain lengths. (b) The frequency and N_P dependence of the ratio (denoted "R") $G'(\omega)/G'_{pol}$ and the difference (denoted "D") $G'(\omega) - G'_{pol}$.

its terminal relaxation regime when the $G'(\omega)$ is still in its plateau regime. In sum, it is evident that the behavior of $G'(\omega)$ observed for $\phi = 0.5$ can neither quantitatively nor qualitatively be accounted by the behavior of $G'_{pol}(\omega)$. We do note, however, that the particle-induced change in the polymer dynamics does by itself lead to a significant enhancement in the viscoelastic properties. The latter is clearly evident in the inset to Figure 7a which presents a comparison of $G'_{pol}(\phi = 0.5)$ with $G'_{pol}(\phi = 0.007)$ to demonstrates the order of magnitude enhancement arising due to this effect. These observations conclusively demonstrate that while change in polymer dynamics plays an important role, the viscoelastic properties observed at higher loadings arise primarily from a particle-induced stress mechanism.

At lower loadings we suggested that a second source of enhancement in $G'(\omega)$ arises from the particle-induced distortion in the elastic strain field. To examine the role of this contribution, in Figure 7b we consider the magnitude and the frequency dependence of the ratio $G'(\omega)/G'_{pol}(\omega)$ (denoted "R" in the figure) for the different polymers. We observe (to within numerical errors) that the particle-induced enhancement asymptotes to an almost constant, N_P-independent value at high frequencies. The latter behavior is similar to the observations at lower particle loadings and is consistent with the expectations the strain field distortion mechanism. However, the main differences arise at lower frequencies where we observe that the magnitude of the relative enhancement grows to a significantly large, N_P-dependent value. In contrast, however, the difference $G'(\omega) - G'_{pol}(\omega)$ (denoted "D") appears to approach a N_P-independent value at the lower frequencies ω. The latter features contrast with the expectations from simple continuum theories,[33−36] which typically posit that $G'(\omega) = G'_{pol}(\omega)f(\phi,\omega)$. While the unknown stress transfer mechanism between the polymer and the particle can in principle lead to a complicated frequency dependence for the effective modulus, we believe that the enhancements observed at low frequency are unlikely to be accountable by this mechanism. In sum, the above results suggests that while the perspective of an effective elastic property of the composite can account for the high-frequency enhancements, the latter cannot rationalize the observed low-frequency viscoelastic behavior.

We suggest that the enhancement in modulus can be rationalized as arising from jamming of the particles. The latter arises when the motion of some or all the degrees of freedom of the particles are caged by the other particles, effectively slowing down their dynamics (rotational or translational) to a time scale related to the "cage-opening" process.[62,63] In the time intervening between equilibration within the cage and the escape from the cage, the particle dynamics is effectively frozen. An application of strain to such a jammed system leads to a short time (high ω) relaxation arising from the equilibration within the cage, followed by plateau in the relaxation until the cage opening time scale, beyond which the relaxation proceeds in a normal manner.[41] In the context of hard-sphere colloids, the latter phenomenon manifests at loadings near the glass transition $\phi_g = 0.58$. In contrast, in anisotropic particles such as platelets similar jamming effects can impede the rotational dynamics of the particles at much lower loadings.[56,64] Moreover, depending on the proximity to the glass transition, the cage-opening time scale in such jammed states can be orders of magnitude larger than the fundamental time scales governing particle motion.[62,63]

We suggest that the plateau and the enhancement in moduli observed in the low-frequency regime of the viscoelastic behavior arises from the caging dynamics of the particle and its associated plateau modulus. We offer two indirect evidences corroborating this claim. The first relates to the order of magnitude of the elastic modulus expected due to jamming. The latter can be estimated using a recent prediction of the elastic moduli (in units of k_BT) near the hard-sphere glass transition:[63]

$$G'_{jam} = 0.00032\phi \frac{1}{(2R)^3}\exp(26\phi) \qquad (5)$$

At a volume fraction of $\phi = 0.5$, eq 5 predicts $G'_{jam} = 0.56$, a number whose order of magnitude is consistent with the enhancement in moduli observed at low frequencies (the low-frequency asymptote of the "D" curve in Figure 7b). Since the above source of elasticity arises from the thermal energy arising from the localization of the particle in a cage, the resulting modulus is independent of the matrix fluid properties.[41,63] The latter feature is again consistent with the N_P independence of our results at lower frequencies.

The second evidence we present relates to the nature of the particle dynamics themselves. Shown in Figure 8a,b are the time-dependent mean-squared displacements (MSD) of the particles at different loadings for $N_P = 8$ and $N_P = 96$ matrices. It is evident that for a loading of $\phi = 0.5$ the MSDs of the particles show a qualitatively different behavior compared to

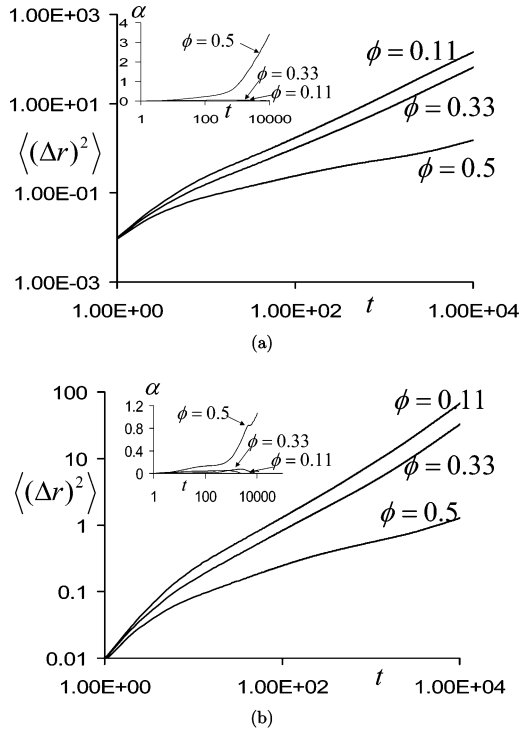

Figure 8. Mean-squared particle displacements $\langle(\Delta \mathbf{r})^2\rangle$ and the non-Gaussian parameter $\alpha(t)$ (defined in the text) as a function of time t: (a) $N_P = 8$; (b) $N_P = 96$.

the other loadings. We observe that the initial dynamics of the particle is followed by an extremely slow intermediate regime indicative of the "trapped" caging regime. Another evidence that our particles indeed display caged dynamics is provided by a characterization of the degree to which the distribution of particle displacements differs from a Gaussian distribution. The latter is typically quantified by the non-Gaussian parameter $\alpha(t)$ defined as[65−67]

$$\alpha(t) = \frac{3\langle[\mathbf{r}_i(t) - \mathbf{r}_i(0)]^4\rangle}{5\langle[\mathbf{r}_i(t) - \mathbf{r}_i(0)]^2\rangle^2} - 1 \qquad (6)$$

where $\mathbf{r}_i(t)$ denotes the position of particle i at a time t. In the insets to Figure 8 are displayed the $\alpha(t)$ computed from the statistics of the displacements of the particles. It is evident that deviations from Gaussian displacements are practically zero at dilute volume fractions, suggesting a regular diffusive dynamical behavior. However, upon increase in the volume fraction to $\phi = 0.5$, $\alpha(t)$ displays a pronounced increase in the plateau regime, again strongly indicative of heterogeneous nature of the particle dynamics.

In principle, it is possible to estimate the caging time scale over which the plateau in $G'(\omega)$ is expected to persist by examining the onset of normal Fickian diffusion in the particle dynamics and/or the time scale which $\alpha(t)$ starts to decrease. Within the time scales probed in our simulation, we were not able to access either of these regimes. We can only suggest that the cage breaking time scale τ_{cage} is such that $\tau_{cage} > 10\,000$, and consequently the plateau due to the particle caging should extend at least up to $\omega \approx 6 \times 10^{-4}$.

In sum, our results demonstrate that qualitatively new aspects of polymer and particle dynamics manifest at the higher particle loading of $\phi = 0.5$. On one hand, the polymer dynamics exhibits entanglement-like behavior (arising from the temporary "cross-links" generated by the particle). The latter effects lead to a significant quantitative contribution to the low- and high-frequency viscoelastic behavior. On the other hand, the particle dynamics exhibits evidence of jamming behavior. Analysis of the viscoelastic behavior strongly suggests that the latter is responsible for the plateau observed in the $G'(\omega)$ of our oscillatory shear simulations.

C. Discussion. The simulation results presented in the previous sections suggest the following picture for the linear viscoelastic properties of our model PNC systems: At low particle loadings the enhancement in modulus arises primarily through the particle-induced effects on the polymer dynamics. At higher particle loadings, while the preceding mechanism is still present (and in a more enhanced manner), the overall low-frequency response is dominated by the particle jamming effects. In the next section, we address the generality of this picture and its connection to other proposals presented in the literature.

4. Discussion: Jamming vs Transient Networks

We recall that at the outset two hypothesis for the rheological behavior of PNCs were noted from the literature, viz., the polymer transient network mechanism and the particle jamming effects. In this section we address the question, "is the simulation observations of particle-induced effects on the polymer dynamics a manifestation of transient networks?" We note that the simulation conditions corresponded to only weak changes in polymer mobility near the particles. Consequently, it is not evident what qualitative changes, if any, would result if the particle has a stronger effect on the polymer mobilities. However, because of the computational times entailed, a direct probe of this regime is not possible in our simulations. In this section, we develop a schematic, but exactly solvable model for polymer dynamics that enables us to identify the qualitative features of G'_{pol} for the case where the particle has a stronger effect on the polymer mobilities. Subsequently, we use the $G'_{pol}(\omega)$ to comment on the expected behavior for $G'(\omega)$.

A. Dynamically Quenched Rouse Model. We consider an exactly solvable toy Rouse model to describe the stress relaxation contribution arising from the polymer matrix chains in the PNC system. We hypothesize that the polymer segments in contact with the particle experience a reduced mobility which impacts their stress relaxations. On the basis of this, we make an analogy between the dynamics of the polymer chains in the PNC system with the dynamics of noninteracting polymer chains (in the absence of any particles) with a heterogeneous distribution of segmental mobilities. Explicitly, if ν denotes the average number of bridges formed by a polymer (i.e., a portion of the polymer chain which simultaneous contacts two particles) and d the average interparticle distance in the actual PNC system, our model system is assumed to contain polymer chains which have on an average ν pairs of slow segments with the elements of the pair being separated on an average by d segments each. Moreoever, for the slow segments the relaxation times are assumed to be enhanced to $A\tau_0$, where τ_0 is the bare relaxation time of the segment and $A \geq 1$.

To detail the construction of matrix chains with the above characteristics, consider the first of the ν "entanglements". We generate the number of segments in this entanglement through a Poisson distribution with a mean d. The ends of this entanglement strands are then assigned the mobility ξ_0/A. Subsequently, we consider the second entanglement and repeat the process until all the ν entanglements have been assigned their strand lengths. The different strands are then stitched together to form the interior of the chain. Now, we generate two strands randomly such that the total number of segments in such strands equal the left over chain segments (i.e., the

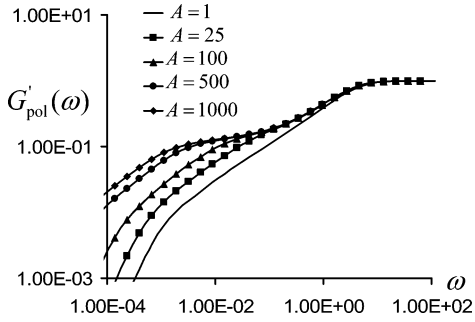

Figure 9. $G'_{pol}(\omega)$ for the schematic Rouse model. The parameters correspond to $\nu = 10$, $d = 3$, and $N_P = 96$. The curve $A = 1$ corresponds to the response of a pure, unperturbed polymer.

difference between N_P and the sum of all segments in the entanglement strands). The polymer chain is then formed with the last two strands forming the two ends of the chain and the entanglements forming the central portion of the chain. In the unlikely, albeit statistically possible, event that the number of segments in the entanglement strands exceed N_P, we randomly discard entanglement strands until the total number of segments in them is less than or equal to the chain length N_P.

In principle, it is possible to utilize an ensemble of the above chains in a dynamical simulation to determine their stress relaxation behavior. However, such an effort proves cumbersome, especially in regimes where there is a significant particle-induced reduction in mobility, i.e., $A \gg 1$. Instead, we use a more direct and exact approach, which involves a direct solution for the averaged dynamic modulus $G(t)$ for an ensemble of Rouse chains with random bead mobilities. The latter uses the properties of random matrices and has been detailed in Dean[71] (and also in Rubinstein and Colby[72]), and we eschew repeating the details here. The total computation time for a single such calculation was less than a minute on a single processor personal computer.

We note here that the above model is only schematic, since in reality the mobilities of the beads are not quenched values and the slow beads can move and can actually become fast beads. Second, in the case where $A \gg 1$, it is more likely that the overall matrix is characterized by a heterogeneous dynamics spectrum (with a few chains forming the network). In such cases, the discussion below is applicable only to the networked chains. Despite these simplifications, the model provides a simplistic framework to understand the qualitative influence of physical parameters upon the viscoelastic response $G'_{pol}(\omega)$.

We use the above model to address the following question: "what is the qualitative impact of a strong reduction in segment mobility?" We consider a scenario of fixed particle concentration (thereby fixing ν and d) and probe the effect of the parameter A upon $G'_{pol}(\omega)$. In Figure 9 we display the results for $G'_{pol}(\omega)$ from the above model for a fixed N_P and for four different values of the reduction in mobility, A. For $A = 25$, we observe that $G'_{pol}(\omega)$ exhibits qualitatively the same relaxation behavior as an unperturbed polymer matrix but with quantitatively enhanced values. This behavior is similar to the characteristics we observed in our simulation results for low loadings and suggests the utility of the schematic model to capture the main features of $G'_{pol}(\omega)$. With a further increase in A, we observe that the relaxation dynamics of $G'_{pol}(\omega)$ is substantially slowed, such that at $A = 500$ we observe a clear plateau in $G'_{pol}(\omega)$. Further increase in A extends this plateau regime to lower frequencies while retaining the same constant value of the plateau modulus.

The above results confirm the picture of "strong" transient networks proposed in the literature[18,19,24,25] and connects it to the "weak" transient networks of our simulations. When the particle-induced effects on the mobility are weak (such as in our simulations), the effect on $G'_{pol}(\omega)$ is observed to be quantitative rather than qualitative ("weak" network). However, when the particle effects exceed a critical value, the particles act like a cross-link for the polymer ("strong" network) and a true plateau develops in $G'_{pol}(\omega)$. The latter occurs when the particle-induced time scale $A\tau_0$ is larger than the time scale of all other relaxation processes happening in the chain. An upper bound for the latter can be obtained by using the longest relaxation time of the chain, or $A \gtrsim N_P^2$. In such cases, the plateau modulus is expected to depend only on the number of cross-links (i.e., the parameter ν) and indeed becomes independent of the value of A. The plateau regime extends up to a frequency $\omega = (A\tau_0)^{-1}$, beyond which the polymer relaxes by a regular Rouse spectrum.

Overall, it is evident that a significant reduction in polymer mobility is needed for the formation of a "strong" polymer network. In real situations, we believe that a "weak" network may be observed for dynamically flexible polymers with low glass transition temperatures, like for instance PDMS, where one can expect only a weak slowing down of segmental dynamics at polymer−solid interface. In contrast, the "strong" case may more likely correspond to a rigid polymer with high isomeric rotational barriers for which one can expect dramatic retardation of segmental dynamics near the interface. However, depending on the particle's influence on the polymer mobilities, a spectrum of networks ranging from "weak" to "strong" is possible. As noted earlier, the enhancements in elasticity resulting in the weaker networks can still be substantial compared to the unperturbed polymer matrix.

B. Transient Networks or Particle Interactions? We can combine the results of our simulations and the insights from the above model to suggest the following general picture for the viscoelastic properties of polymer−nanoparticle composites containing spherical particles. For low loadings, the transient network mechanism is expected to dominate the viscoelastic response, and we expect that $G'(\omega)$ for the composite to be quantitatively identical to $G'_{pol}(\omega)$ at low frequencies. We speculatively suggest that at such regimes the high-frequency response is influenced by the distortions in strain field arising from the presence of the particles. For higher loadings, the interplay between the G'_{pol} arising from a strong network and G'_{jam} is more subtle and requires detailed knowledge of the polymer conformations at a given particle loading. However, in a subsequent article we present the results of polymer self-consistent-field theory based calculations,[68] which confirms our simulation results above. Together they suggest that for volume fractions $\phi \gtrsim 0.45$, despite the substantial nature of the transient network contribution, the low-frequency response is still dominated by the particle jamming effects noted in our simulations.

5. Summary

In this work, we have used simulations of the simplest model of polymer nanocomposites to identify the mechanisms underlying their viscoelastic behavior. Specifically, we have focused on the linear elasticity of the modulus ($G'(\omega)$) and the manner in which the polymer and the particle contributions can rationalize its shape and magnitudes. Our simulations suggest that $G'(\omega)$ of the PNC system is influenced by a variety of effects whose relative influences are controlled by both the loading of the particles and the frequency at which the responses are probed. Overall, the particles can contribute to $G'(\omega)$ in three

different ways: (i) The particle-induced effects on the polymer segments can modify the dynamics and relaxation spectrum of the polymers. (ii) Particle jamming effects can lead to slow relaxations and substantial enhancements in elasticity. (iii) The strain field distortion caused by the presence of rigid inclusions can affect the overall modulus of the composite.

In our model system containing spherical nanofillers well dispersed in polymer matrices, we were able to identify the relative influences of the above effects. These results suggested that for a wide range of particle loadings the low frequency response is dominated by the particle-induced changes in polymer dynamics. Only at very high loadings does modulus arising from the particle jamming effects dominate the overall viscoelastic behavior. One of the main contributions of our work is to suggest that a true or a "strong" network is not a necessity for the overall properties of the composite to be significantly enhanced. Indeed, simple scaling arguments suggest that a substantial reduction in polymer mobility is needed for a true polymer network to form. Rather, the viscoelastic spectrum can still be both quantitatively and qualitatively modified in cases where a "weak" network forms.

While our hypothesis was motivated by experimental results probing the behavior of polymer chains near surfaces,[26−29] the origins of such effects have not been fully resolved. For instance, polymer−particle enthalpic interactions have been speculated to lead to an enhanced polymer density which leads to a concomitant reductions in the near-surface mobility of the polymers.[26−29] However, recent simulations suggest that the latter effects can only lead to very small changes in the near-surface mobility of polymer melts.[30] Alternatively, impenetrable and/heterogeneous surfaces[30] can lead to large barriers for segmental relaxation and can lead to significant reductions in mobility. Our simulations suggest that controlling these effects will prove fruitful as a means to control the properties of the composite themselves.

Care must be taken in generalizing the implications of our results to the experimental situations. Most experiments have involved anisotropic fillers dispersed in polymeric matrices.[17] Moreover, the particles themselves are most often in a directly aggregated state. Neither of these effects are accounted in our simulations. Furthermore, entanglement of polymers (neglected in our model and simulations) will certainly lead to more relaxation regimes not captured in our results for the linear viscoelasticity. Despite these drawbacks, some of the insights gained through the analysis and the computer simulations still provide a useful starting point for developing mechanistic explanations for experiments. For instance, we note that many of the polymer effects noted in our simulations will still be semiquantitatively accurate (when accounted for the larger surface areas of anisotropic fillers) even in the case where anisotropic fillers are involved. In contrast, the elasticity resulting from particle jamming effects are profoundly different when either anisotropy or aggregation can occur.[69] The latter can be expected to lead to nontrivial shifts in the volume fractions at which particle effects dominate. Our future studies will focus on such issues.

Acknowledgment. We thank Profs. K. Schweizer, R. Krishnamoorti, D. R. Paul, and P. F. Green for patiently educating us on the subtleties of polymer nanocomposites, which helped shape the ideas presented in this work. This work was supported in part by a Sloan Fellowship by the Alfred P. Sloan Foundation, by a grant from Robert A. Welch Foundation, and by the National Science Foundation under Award NSF DMR-02-04199. We also acknowledge a generous grant of computer time in Texas Advanced Computing Center where all the computations reported in this article were performed.

Appendix. Simulation Model and Parameters

1. Simulation Approach. Dissipative particle dynamics (DPD)[47] and the variant we use[48] are in actuality molecular dynamics simulation approach with a specific choice of the forces. Both the particles and the polymer segments are represented by their positions and translational velocities. In addition, because of the presence of shear forces on the particles, the particles are also ascribed a rotational degree of freedom. The time evolution of these degrees of freedom is governed by the following equations of motion:

$$\frac{\mathrm{d}\mathbf{r}_i}{\mathrm{d}t} = \mathbf{v}_i; \quad m_i \frac{\mathrm{d}\mathbf{v}_i}{\mathrm{d}t} = \sum_{j\neq i} \mathbf{F}_{ij}; \quad I_i \frac{\mathrm{d}\omega_i}{\mathrm{d}t} = -\sum_{j\neq i} \lambda_{ij} \mathbf{r}_{ij} \times \mathbf{F}_{ij} \qquad \text{(A1)}$$

In the above equation, $\mathbf{r}_i$,$\mathbf{v}_i$, and ω_i denote the position and linear and angular velocities of the particle (i is applicable to both the polymer segment and the particle). The mass and the moment of inertia of particle are denoted as m_i and I_i, while $\mathbf{r}_{ij}$ and $\mathbf{F}_{ij}$ denote the respectively relative separations and forces between particles i and j. The factor λ_{ij} is phenomenologically included in the angular momentum equation to account for the asymmetry in the sizes of the particles and the resulting asymmetries in the torques due to the point of application of the forces. In the previous work,[48] we adopted a simple functional form for λ_{ij} as $\lambda_{ij} = R_i/R_i + R_j$, where R_i and R_j denote the radii of the particles i and j, respectively. Note, by definition, $\lambda_{ji} = 1 - \lambda_{ij}$, which preserves the conservation of angular momentum. In this work we directly incorporate the asymmetric sizes of the polymer segments and the particle by setting $\lambda_{ij} = 1$ if i is a particle and j is a polymer segment. This also eliminates the need to account for the rotational degree of freedom for the polymer segments.

The force $\mathbf{F}_{ij}$ has four components: $\mathbf{F}_{ij} = \mathbf{F}_{ij}^{(\mathrm{C})} + \mathbf{F}_{ij}^{(\mathrm{T})} + \mathbf{F}_{ij}^{(\mathrm{R})} + \tilde{\mathbf{F}}_{ij}$, where the forces $\mathbf{F}_{ij}^{(\mathrm{C})}$, $\mathbf{F}_{ij}^{(\mathrm{T})}$, $\mathbf{F}_{ij}^{(R)}$, and $\mathbf{F}_{ij}$ represent the generalizations of the DPD intermolecular interactions, velocity-dependent drag forces, rotational drag forces, and the random forces maintaining the temperature of the system. We adopt the following form for $\mathbf{F}_{ij}^{(T)} = -\gamma_{ij}[f(r)]^2[\mathbf{I} + \mathbf{e}_{ij}\mathbf{e}_{ij}]\cdot\mathbf{v}_{ij}$, where $\mathbf{e}_{ij}$ denotes the unit vector along the line of centers joining the particles i and j and

$$f(r) = \begin{cases} 1 - \dfrac{r_{ij}}{r_{ij}^C} & r \le r_{ij}^C \\ 0 & r \ge r_{ij}^C \end{cases} \qquad \text{(A2)}$$

In the above equations r_{ij}^C physically denotes a cutoff distance for the forces between the components i and j beyond which the forces are set to zero. The constant γ_{ij} is a phenomenological constant quantifying the strength of the drag forces. The rotational force is of the form $\mathbf{F}_{ij}^{(R)} = -\gamma_{ij}[f(r)]^2[\mathbf{I} + \mathbf{e}_{ij}\mathbf{e}_{ij}]\cdot[\mathbf{r}_{ij} \times (\lambda_{ij}\omega_i + \lambda_{ji}\omega_j)]$. The functional form of the corresponding stochastic force is fixed by fluctuation−dissipation theorem and is identical to our earlier work.

In addition to above generalized drag forces, we also generalize the interaction forces $\mathbf{F}_{ij}^{(C)}$ to account for the different natures of particle (hard) and polymer segment (soft) components. For the nonbonded part of the polymer−polymer interactions, we retain the original DPD form of soft repulsive potentials:[47,54] $\mathbf{F}_{SS}^{(C1)}(\mathbf{r}) = af(r)\mathbf{e}_{SS}$, where a represents the

strength of segment−segment interactions. The connectivity of the polymer is incorporated through a FENE potential of the form[70]

$$\mathbf{F}_{SS}^{(C2)}(\mathbf{r}) = \frac{H}{1 - \left(\frac{r}{b}\right)^2}\mathbf{r} \tag{A3}$$

where H denotes the spring constant and b represents the maximum extension length of a polymer bond. For the segment−particle and particle−particle interactions we used Lennard-Jones interaction potentials:

$$\mathbf{F}_{SC}^{(C)}(\mathbf{r}) = \begin{cases} \dfrac{12\epsilon_{SC}\sigma_{SC}^{\ 6}}{r^8}\left(1 - \dfrac{\sigma_{SC}^{\ 6}}{r^6}\right)\mathbf{r} & r < r_{SC} \\ 0 & r > r_{SC} \end{cases};$$

$$\mathbf{F}_{CC}^{(C)}(\mathbf{r}) = \begin{cases} \dfrac{12\epsilon_{CC}\sigma_{CC}^{\ 6}}{r^8}\left(1 - \dfrac{\sigma_{CC}^{\ 6}}{r^6}\right)\mathbf{r} & r < r_{CC} \\ 0 & r > r_{CC} \end{cases} \tag{A4}$$

The cutoff radii r_{SS}, r_{CC}, and r_{SC} appearing in the above interaction potentials were all chosen to be the same values as in the drag forces.

2. Numerical Integration. Simulation of the motion of the colloid and polymer segment molecules involves a numerical integration of eqs A1 for the forces specified above. For this purpose, we have utilized a modified velocity Verlet numerical scheme suggested first by Groot and Warren.[47] This scheme is identical to that detailed in our previous article, to which we refer the interested reader.[48] As outlined in our earlier article, we used a modified version of linked-list algorithm to expedite the calculation of forces.

3. Simulation Parameters. The cutoff radii for the segment−segment, segment−colloid, and colloid−colloid interactions were chosen to be the following values: $r_{SS} = 1$, $r_{SC} = 3$, and $r_{CC} = 5$. Note that the polymer segment moieties in our simulations are DPD molecules and represent coarse-grained representations of the real segment units. Consequently, our simulations correspond to physical systems wherein the colloids are possibly at least an order of magnitude larger than the segment units. Most of these parametrizations and numbers are identical to that chosen in our earlier work on colloidal particles in simple fluids. Therein, we demonstrated that this size disparity suffices to capture hydrodynamical phenomena relevant to macroscopic suspensions.

In our simulation, we fixed the strength of the segment−segment interaction $a = 250$ and their friction parameters $\gamma_{SS} = 4.5$. The segment−particle parameters were fixed at $\gamma_{SC} = \gamma_{CC} = 450.0$. The latter physically represents the enhanced drag (i.e., reduced mobilities) the polymer segments experience when near the particles. The simulation results were found to be not sensitive to the value of parameter γ_{CC} (particle−particle drag coefficient). The L−J parameters for particle−particle and particle−segment interactions where chosen as $\epsilon_{CC} = 110.0$, $\sigma_{CC} = 4.45$, $\epsilon_{CS} = 3.0$, and $\sigma_{CS} = 2.45$. The spring constant for the FENE springs was chosen as $H = 1.0$ and the maximum extensibility of the springs $b = 3.0$. Masses were expressed in the units of mass of the polymer segment $m_s = 1$ and the energy scale $k_BT = 1$. The mass of the colloid particle was chosen proportionately to its volume as $m_C = 196.0$, and the moment of inertia of the colloid particle was fixed at $I_C = 491.0$.

All our simulations were carried out in a cubic box with periodic boundary conditions. Setting up the initial configuration of our system requires some care, and we use a "scale-up" approach outlined in our earlier article.[48] We studied two densities of the polymeric fluids: (i) a "high-density" matrix containing 15 360 polymer segment units in the box, which in the absence of colloidal particles corresponds to a number density of $\rho_p = 1.53$ at $N_p = 48$; (ii) a "low-density" system, containing 7680 segment units in the box, which corresponds to $\rho_p = 1.0$ at $N_p = 48$. The qualitative features of all the results were identical between these systems, and so we have just presented the low-density system in the main text. To keep the properties of the DPD polymer matrix close to the same value in all the runs, we used different cell sizes for the different runs. The cell sizes were chosen on the basis of the constraint that the pressure at equilibrium was the same constant value for all runs. The constraint of constant pressure led to cell sizes which varied in the range of 19−24 segment size units between the dilute and the concentrated particle regimes.

4. Oscillatory Shear. An approach commonly employed to determine the linear viscoelastic properties in molecular dynamics simulations involves the use of Kubo formula relating the dynamic modulii to the stress−stress autocorrelation functions.[44,52] However, recent work by Barrat and co-workers has demonstrated that such an approach is extremely error prone (unless long trajectories are used) and has cautioned against its usage for systems involving polymeric components.[53] Consequently, to simulate oscillatory shear, we have use a direct nonequilibrium method outlined in Allen and Tildesley.[54] This entails a simulation with an additional force in the x-direction along with time dependent Lees−Edwards boundary condition. For instance, the equation of motion for x velocities of particle i is now modified as

$$m_i \frac{\mathrm{d}v_{ix}}{\mathrm{d}t} = F_{ix} + m_i r_{iy} \frac{\mathrm{d}^2\gamma(t)}{\mathrm{d}t^2} \tag{A5}$$

where for the oscillatory strain considered, $\gamma(t) = A_\omega[1 - \cos(\omega t)]$. The simulation results presented in the main text correspond to a strain $A_\omega = 0.1$ and frequencies $\omega = 2\pi/T_\omega$, where $T_\omega = \{10^1;10^2;10^3;10^4\}$.

5. Polymer Normal Modes. Many key results in the main text rely upon the behavior of the relaxation spectrum of the normal modes of the individual polymer chains. Such normal modes are by and large useful if the intrachain correlations in the polymer matrix are much higher than the interchain correlations—an assumption underlying many polymer melt theories.[56] In such cases, one can identify the dynamical characteristics of the polymer matrix by studying the relaxation characteristics of a single chain. Since we used a FENE polymer matrix, we determined the normal modes and their relaxations specifically for the different polymer chains used in our simulations. In the following we briefly describe the manner in which the normal modes and their relaxation spectra were discerned.

Using the trajectories generated during our equilibrium simulations, at a given time, the position of the center of mass of a polymer chain was determined as $\mathbf{r}_0 = \sum_{i=1}^{N_p}\mathbf{r}_i$, where $\mathbf{r}_i$ denotes the (vectorial) positions of the segment i on the chain. Using $\mathbf{r}_0$, we constructed a symmetric matrix $\mathbf{R}$, the elements of which are given by

$$R_{\alpha\beta ij} = \langle (r_0^\alpha - r_i^\alpha)(r_0^\beta - r_j^\beta)\rangle \tag{A6}$$

where i and j represent the segment indices and α and β represent the spatial coordinates ($\alpha, \beta = x, y, z$). The notation $\langle ... \rangle$ is used to represent an average which extends over all chains

in the system and over the entire equilibrium runs. The above matrix quantifies in an averaged manner the correlation of the position of the segments relative to the center of mass in the polymer chains.

For homogeneous, isotropic systems, $R_{\alpha\beta ij}$ for $\alpha \neq \beta$ is negligible compared to $R_{\alpha\beta ij}$ for $\alpha = \beta$. Whence we used the averaged matrix $R_{ij} = {}^1/_3\sum_\alpha R_{\alpha\alpha ij}$ to determine the normal modes $\mathbf{X}_p$. The latter were determined as the eigenvectors of the matrix R_{ij}. Using these normal modes, we determined their relaxation spectra $M(t)$ as

$$\langle X_{\alpha i}(t=0)X_{\beta j}(t=t)\rangle = \lambda_i \delta_{\alpha\beta}\delta_{ij}M_i(t) \qquad \text{(A7)}$$

where λ_i denotes the eigenvalue corresponding to the normal mode i and $\langle X_{\alpha i}(t=0)X_{\beta j}(t=0)\rangle = \lambda_i \delta_{\alpha\beta}\delta_{ij}$.

References and Notes

(1) Boisvert, J. P.; et al. *Colloids Surf., A* **2001**, *187*, 178.
(2) Schaller, C.; et al. *Eur. Phys. J. E* **2001**, *6*, 365.
(3) Russel, W. B.; Saville, D. A.; Schowalter, W. R. *Colloidal Dispersions*; Cambridge University Press: New York, 1999.
(4) Du, F. M.; et al. *J. Polym. Sci., Part B: Polym. Phys.* **2003**, *41*, 3333.
(5) Chapman, R.; Mulvaney, P. *Chem. Phys. Lett.* **2001**, *349*, 348.
(6) Yoon, P. J.; Fornes, T. D.; Paul, D. R. *Polymer* **2002**, *43*, 6727.
(7) Bolhuis, P. G.; Louis, A. A.; Hansen, J. P. *Phys. Rev. Lett.* **2002**, *89*, 128302.
(8) Ramakrishnan, S.; et al. *Langmuir* **2003**, *19*, 5128.
(9) Surve, M.; Pryamitsyn, V. A.; Ganesan, V. *J. Chem. Phys.* **2004**, *122*, 154901.
(10) Hooper, J. B.; et al. *J. Chem. Phys.* **2004**, *121*, 6986.
(11) Larson, R. G. *The Structure and Rheology of Complex Fluids*; Oxford University Press: New York, 1999.
(12) Mackay, M. E.; et al. *Nat. Mater.* **2003**, *2*, 762.
(13) Schmidt, G.; Malwitz, M. M. *Curr. Opin. Colloid Interface Sci.* **2003**, *8*, 103.
(14) Krishnamoorti, R.; Yurekli, K. *Curr. Opin. Colloid Interface Sci.* **2001**, *6*, 464.
(15) Du, F.; et al. *Macromolecules* **2001**, *37*, 9048.
(16) Schmidt, G.; et al. *Macromolecules* **2000**, *33*, 7219.
(17) Krishnamoorti, R.; Giannelis, E. P. *Macromolecules* **1997**, *30*, 4097.
(18) Zhang, Q.; Archer, L. A. *Langmuir* **2002**, *18*, 10435.
(19) Zhang, Q.; Archer, L. A. *Macromolecules* **2004**, *37*, 1928.
(20) Solomon, M. J.; et al. *Macromolecules* **2001**, *34*, 1864.
(21) Galgali, G.; Ramesh, C.; Lele, A. *Macromolecules* **2001**, *34*, 852.
(22) Lozano, K.; et al. *J. Appl. Polym. Sci.* **2001**, *80*, 1162.
(23) Potschke, P.; et al. *Polymer* **2002**, *43*, 3247.
(24) Salaniwal, S.; Kumar, S. K.; Douglas, J. F. *Phys. Rev. Lett.* **2002**, *89*, 258301.
(25) Sternstein, S. S.; Zhu, A. J. *Macromolecules* **2002**, *35*, 7262.
(26) Granick, S.; et al. *J. Polym. Sci., Part B: Polym. Phys.* **2003**, *41*, 2755.
(27) Pu, Y.; et al. *Phys. Rev. Lett.* **2001**, *87*, 206101.
(28) Masson, J. L.; Green, P. F. *Phys. Rev. E* **2002**, *65*, 031806.
(29) Keddie, J. L.; et al. *Faraday Discuss.* **1994**, *98*, 219.
(30) Smith, G. D.; Bedrov, D.; Borodin, O. *Phys. Rev. Lett.* **2003**, *90*, 226103.
(31) Eilers, H. *Kolloid-Z.* **1941**, *97*, 313. Blatz, P. J. *Ind. Eng. Chem.* **1956**, *48*, 727.
(32) Bicerano, J.; Douglas, J. F.; Brune, D. A. *J. Macromol. Sci., Rev. Macromol. Chem. Phys. C* **1999**, *39*, 561.
(33) Luo, J. J.; Daniel, M. M. *Compos. Sci. Technol.* **2003**, *63*, 1607.
(34) Fornes, T. D.; Pa, D. R. *Polymer* **2003**, *44*, 4993.
(35) Smallwood, H. M. *J. Appl. Phys.* **1944**, *15*, 758.
(36) Fisher, F. T.; Brinson, L. C. *Compos. Sci. Technol.* **2001**, *61*, 731.
(37) Kirkpatrick, S. *Rev. Mod. Phys.* **1973**, *45*, 574.
(38) Janzen, J. *J. Appl. Phys.* **1975**, *46*, 966.
(39) Heyes, D. M.; Melrose, J. R. *J. Phys. A* **1988**, *21*, 4075.
(40) Megen van, W.; Underwood, S. M. *J. Chem. Phys.* **1989**, *91*, 552.
(41) Mason, T. G.; Weitz, D. A. *Phys. Rev. Lett.* **1995**, *75*, 2770.
(42) Brady, J. F. *J. Chem. Phys.* **1993**, *98*, 3335.
(43) Lionberger; R. A.; Russel, W. B. *J. Rheol.* **1997**, *41*, 399.
(44) Smith, G. D.; et al. *J. Chem. Phys.* **2002**, *117*, 9478.
(45) Starr, F. W.; et al. *J. Chem. Phys.* **2003**, *119*, 1777.
(46) Desai, T.; Keblinski, P.; Kumar, S. K. *J. Chem. Phys.* **2005**, *122*, 134910.
(47) Groot, R. D.; Warren, P. B. *J. Chem. Phys.* **1997**, *107*, 4423.
(48) Pryamitsyn, V. A.; Ganesan, V. *J. Chem. Phys.* **2005**, *122*, 104906.
(49) Espanol, P. *Europhys. Lett.* **1997**, *39*, 605.
(50) Espanol, P. *Phys. Rev. E* **1998**, *57*, 2930.
(51) Groot, R. D.; Agterof, W. G. M. *Macromolecules* **1995**, *28*, 6284.
(52) Sen, S.; Kumar, S. K.; Keblinski, P. *Macromolecules* **2005**, *38*, 650.
(53) Vladkov, M.; Barrat, J. L. cond-mat/0507229 (preprint, 2005).
(54) Allen, M. P.; Tildesley, D. J. *Computer Simulation of Liquids*; Oxford University Press: New York, 1989.
(55) Spenley, N. A. *Europhys. Lett.* **2000**, *49*, 534.
(56) Doi, M.; Edwards, S. F. *The Theory of Polymer Dynamics;* Oxford University Press: Oxford, UK, 1986.
(57) Kremer, K.; Grest, G. S. *J. Chem. Phys.* **1990**, *92*, 5057.
(58) Hess, W. *Macromolecules* **1988**, *21*, 2620.
(59) Palmer, G.; et al. *Phys. Rev. Lett.* **1984**, *53* 958.
(60) Dominics, D.; Orland, H.; Lainee, F. *J. Phys., Lett.* **1985**, *46*, L463.
(61) Phillips, J. C. *Rep. Prog. Phys.* **1996**, *59*, 1133.
(62) Schweizer, K. S.; Saltzman, E. J. *J. Chem. Phys.* **2003**, *119*, 1181.
(63) Kobelev, V.; Schweizer, K. S. *Phys. Rev. E* **2005**, *71*, 021401.
(64) Moreno, A. J.; Kob, W. *Europhys. Lett.***2004**, *67*, 820.
(65) Kob, W.; et al. *Phys. Rev. Lett.* **1997**, *79*, 2827.
(66) Kasper, A.; Bartsch, E.; Sillescu, H. *Langmuir* **1998**, *14*, 5004.
(67) Kegel, W. K.; Blaaderen van, A. *Science* **2000**, *287*, 290.
(68) Surve, M.; Pryamitsyn V. A.; Ganesan, V. *Macromolecules*, to be submitted.
(69) Wolthers, W.; et al. *Phys. Rev. E* **1997**, *56*, 5726.
(70) Ottinger, H. C. *Stochastic Processes in Polymeric Fluids: Tools and Examples for Developing Simulation Algorithms*; Springer: Berlin, 1996.
(71) Dean, P. *Proc. Phys. Soc.* **1964**, *84*, 727.
(72) Rubinstein, M.; Colby, R. H. *J. Chem. Phys.* **1988**, *89*, 5291.

MA051841Z